Reconstructing random media. II. Three-dimensional media from two-dimensional cuts

C. L. Y. Yeong and S. Torquato
Department of Civil Engineering and Operations Research and Princeton Materials Institute, Princeton University, Princeton, New Jersey 08540
(Received 31 October 1997)

We report on an investigation concerning the utilization of morphological information obtained from a two-dimensional (2D) slice (thin section) of a random medium to reconstruct the full three-dimensional (3D) medium. We apply a procedure that we developed in an earlier paper that incorporates any set of statistical correlation functions to reconstruct a Fontainebleau sandstone in three dimensions. Since we have available the experimentally determined 3D representation of the sandstone, we can probe the extent to which intrinsically 3D information (such as connectedness) is captured in the reconstruction. We considered reconstructing the sandstone using the two-point probability function and lineal-path function as obtained from 2D cuts (cross sections) of the sample. The reconstructions are able to reproduce accurately certain 3D properties of the pore space, such as the pore-size distribution, the mean survival time of a Brownian particle, and the fluid permeability. The degree of connectedness of the pore space also compares remarkably well with the actual sandstone. However, not surprisingly, visualization of the 3D pore structures reveals that the reconstructions are not perfect. A more refined reconstruction can be produced by incorporating higher-order information at the expense of greater computational cost. Finally, we remark that our reconstruction study sheds light on the nature of information contained in the employed correlation functions. [S1063-651X(98)04807-7]

PACS number(s): 44.30.+v

I. INTRODUCTION

The reconstruction of the structure of three-dimensional (3D) random heterogeneous media, such as porous and composite media, from the information obtained from a two-dimensional (2D) micrograph or image has manifold potential applications. Such reconstructions are of great value in a wide variety of fields, including petroleum engineering, biology, and medicine, because in many cases, only 2D images are available for analysis. An effective reconstruction procedure enables one to generate accurate structures at will, and subsequent analysis can be performed on the image to obtain desired macroscopic properties (e.g., transport, electromagnetic, and mechanical properties) of the media. A successful reconstruction procedure could provide a nondestructive and relatively low-cost means of estimating the macroscopic properties of a heterogeneous medium.

An extensively examined reconstruction approach is the Gaussian filtering method [1–3] which utilizes only the standard two-point probability function (obtainable from small-angle scattering experiments [4]) for reconstruction. These methods use linear and nonlinear filters on Gaussian random fields to match the correlation function in the reconstruction process. Clearly, the conventional two-point correlation function alone may not be adequate to characterize the microstructure of the medium for accurate reconstruction. Moreover, it is difficult to extend Gaussian filtering methods to incorporate other correlation functions for two-phase isotropic media, and practically impossible to extend them to general multiphase and anisotropic media. In many cases, additional correlation functions will be required to capture the structural characteristics of a medium (e.g., see the comments in Ref. [5]). It is therefore desirable that a reconstruction procedure have the ability to incorporate as much crucial microstructural information as possible to capture the salient features of the reference structure.

Recently, Rintoul and Torquato [6] developed a reconstruction procedure which can incorporate any set of correlation functions to reconstruct dispersions of particles. In the first paper of this series [7] (hereafter referred to as paper I), we extended this method to reconstruct D-dimensional random media of *arbitrary* topology by considering digitized representations of the systems. To illustrate the method, we applied it in paper I to reconstruct various 1D and 2D random systems from 1D and 2D representations of them, respectively [7]. Further extension of the method to reconstruct 3D media from 3D representations is straightforward but is not the focus of the present work.

In this paper, we concentrate our attention on using microstructural measures obtained from a 2D slice of the medium to reconstruct the full 3D system. However, the extent to which such structural quantities are able to reproduce intrinsic 3D information, such as the pore-size distribution or, more generally, connectedness of the phases, needs to be closely examined. The purpose of this paper is to carry out such a study. An exploration of this kind can shed light on the nature of the information contained in the morphological quantities that are being implemented. This can help one to identify the appropriate morphological descriptors that can effectively characterize classes of structures in order to generate accurate structures for analysis.

A variety of morphological measures for 3D *isotropic* media are obtainable exactly from 2D planes of the medium in the infinite-volume limit. Thus the determination of these quantities from 2D slices will be the same (apart from small error) as the corresponding quantities determined from the 3D image. These quantities, to name a few, include the vol-

ume fraction ϕ_i of phase i, the specific surface s, the two-point probability function S_2, and the lineal-path function L, all of which will be described in detail later.

For present purposes, we will use the two-point probability function and the lineal-path function to reconstruct a 3D Fontainebleau sandstone sample. We showed in paper I [7] that using a combination of both of these correlation functions is superior to using either of the correlation functions alone. Nonetheless, we will begin by reconstructing the sandstone using only the two-point probability function for purposes of comparison. Subsequently, we will incorporate a combination of *both* the two-point probability function and the lineal-path function as the morphological information for reconstruction. We will then compare the 3D morphological quantities and transport properties (mean survival time and fluid permeability) of the different reconstructions to the corresponding quantities of the 3D representation of the actual sandstone. Although we focus on the two-phase sandstone for purposes of illustration in this paper, we emphasize that our reconstruction procedure is general enough to treat multiphase media [7]. Finally, we graphically display our reconstructions as 3D perspectives of the void space and as surface cuts.

We would like to point out that there are many other reconstruction methods in the literature, especially in the fields of data compression and tomographic reconstruction. These methods, to name a few, include the wavelets or multiwavelets reconstruction and reconstruction from Fourier spectra or power spectral data. However, these procedures are only used for image compression and subsequent expansion of data, problems that are not related to the questions that we are addressing, namely, the treatment of a single or multiple correlation functions as the input data and subsequent reconstruction of the corresponding image. Furthermore, since these methods are not able to target particular morphological correlation functions for reconstruction, they generally cannot give insight into morphological characterization. The aim of our reconstruction procedure is not to produce an exact duplicate of the original image. On the contrary, the intent is to utilize *limited* information (measurable correlation functions) about the random media to reconstruct a family of microstructures that have the same correlation functions.

The outline of the rest of the paper is as follows: In Sec. II, we define and discuss the structural quantities and the macroscopic properties that we will employ in this paper. In Sec. III, we outline briefly the reconstruction procedure for digitized media, and discuss, among others things, how we incorporate the two-point probability function and the lineal-path function as the input information, although the technique is capable of treating any number of correlation functions. In Sec. IV, we apply the procedure to perform 3D reconstructions of the Fontainebleau sandstone sample by utilizing the aforementioned structural information ascertained from 2D cross-sectional images. We also evaluate transport properties of the resultant reconstructions, and compare them to those of the real sandstone. We illustrate our reconstructions as 3D perspectives of the void space and as surface cuts. In Sec. V, we make concluding remarks.

II. MORPHOLOGICAL QUANTITIES AND MACROSCOPIC PROPERTIES

The two-phase random medium is a domain of space $\mathcal{V}(\omega) \in \Re^3$, where the realization ω is taken from some probability space of volume V which is composed of two regions or phases: phase 1, the region $\mathcal{V}_1$ of volume fraction ϕ_1; and phase 2, the region $\mathcal{V}_2$ of volume fraction ϕ_2. Let $\partial\mathcal{V}$ denote the surface or interface between $\mathcal{V}_1$ and $\mathcal{V}_2$. For a given realization ω, the characteristic function $I(\mathbf{x})$ of phase 1 is given by

$$I(\mathbf{x}) = \begin{cases} 1 & \text{if } \mathbf{x} \in \mathcal{V}_1 \\ 0 & \text{if } \mathbf{x} \in \mathcal{V}_2 . \end{cases} \tag{1}$$

The characteristic function $M(\mathbf{x})$ for the interface is defined as

$$M(\mathbf{x}) = |\nabla I(\mathbf{x})|. \tag{2}$$

In this paper, we denote phase 1 as the void or pore phase of the Fontainebleau sandstone, and phase 2 as the material or grain phase.

A. One- and two-point probability functions

For statistically homogeneous media, the simplest morphological measure is the volume fraction ϕ_1 of phase 1, which is the one-point correlation function defined by

$$\phi_1 = \langle I(\mathbf{x}) \rangle, \tag{3}$$

where angular brackets denote an ensemble average. The volume fraction can be interpreted as the probability of finding a point in phase 1. In a digitized medium, ϕ_1 can simply be found by directly counting the number of phase 1 pixels over the whole medium. For simplicity, we will use the term ''pixel'' throughout the paper, with the understanding that we mean ''voxel'' for a pixel in three dimensions.

The specific surface s of a two-phase medium is the area of the two-phase interface per unit total volume of the medium. The inverse quantity s^{-1} is an important characteristic length scale of the medium. The specific surface is itself a one-point correlation function defined by

$$s = \langle M(\mathbf{x}) \rangle. \tag{4}$$

For the 3D digitized media in this study, we evaluate s by directly counting the interfacial area of each three-dimensional pixel belonging to the material phase. For systems that do not have periodic boundary conditions, care is taken to avoid including the system boundary as the interfacial area.

The two-point probability function is defined as

$$S_2(\mathbf{x}_1, \mathbf{x}_2) = \langle I(\mathbf{x}_1) I(\mathbf{x}_2) \rangle, \tag{5}$$

where $\mathbf{x}_1$ and $\mathbf{x}_2$ are two arbitrary points in the system. This can be interpreted as the probability of finding two points at positions $\mathbf{x}_1$ and $\mathbf{x}_2$ both in phase 1. For statistically isotropic media, the two-point probability function depends only on the magnitude of the separation $r = |\mathbf{x}_1 - \mathbf{x}_2|$ between the two points, and therefore can be expressed simply as $S_2(r)$. For all isotropic media without long-range order,

$$S_2(0)=\phi_1 \quad \text{and} \quad \lim_{r\to\infty} S_2(r)=\phi_1^2. \tag{6}$$

In general, we can define the n-point probability function

$$S_n(\mathbf{x}_1,\mathbf{x}_2,\ldots,\mathbf{x}_n)=\langle I(\mathbf{x}_1)I(\mathbf{x}_2)\ldots I(\mathbf{x}_n)\rangle. \tag{7}$$

There are many other n-point correlation functions apart from the n-point probability function, and we refer the reader to Ref. [8] for a thorough review. We note in passing that the two-point function S_2 for porous media is obtainable from small-angle scattering experiments [4].

For a 3D continuum medium, it has been shown that the slope of the two-point probability function of either phase at $r=0$ is related to the specific surface s via the relation [4,9]

$$\left.\frac{dS_2(r)}{dr}\right|_{r=0} = -s/4. \tag{8}$$

For a 3D *digitized* medium, due to the effect of discretization, the slope is instead [7]

$$\left.\frac{dS_2(r)}{dr}\right|_{r=0} = -s/6. \tag{9}$$

It should be emphasized that the two-point probability function cannot distinguish between phase 1 and phase 2 materials since $S_2^{(1)}(r)-\phi_1^2=S_2^{(2)}(r)-\phi_2^2$ (the superscripts denote the phase), nor does it reflect information about the connectedness of the phases.

In evaluating $S_2(r)$ of a digitized medium, the discrete nature arising from the digitization means that the distance r can conveniently be measured in terms of pixels and acquires integral values, with the end points of r located at the pixel centers. Also, it can be shown that when sampled along the direction of rows of pixels, $S_2(r)$ is a linear function between adjacent pixels:

$$S_2(r)=(1-f)\,S_2(i)+f\,S_2(i+1) \quad \text{for } i\leqslant r<i+1, \tag{10}$$

where i is an integer, and $f=r\,\mathrm{mod}1$. Because of this linear property, the evaluation of $S_2(r)$ at integral values of r is sufficient to characterize the structure, and determining it for noninteger values of r is not necessary. Consequently, $S_2(r)$ can be evaluated simply by successively translating a line of r $(=i)$ pixels in length at a distance of one pixel at a time and spanning the whole image, counting the number of successes of the two end points falling in phase 1, and finally dividing the number of successes by the total number of trials. We employed periodic boundary conditions in all reconstructed systems, and therefore the total number of trials is the system size in those cases. For a D-dimensional isotropic system, we sample only along D orthogonal directions in the rows of pixels. It is observed that this sampling procedure can be more accurate, and produces a smoother S_2 profile than that by random sampling (throwing random points into the system), because the former exhaustively incorporates information from every pixel in the entire system. Of course, at additional computational cost, one could sample S_2 in more directions than the orthogonal directions only.

B. Lineal-path function

Another important morphological descriptor of the structure of random media is the lineal-path function $L(\mathbf{x},\mathbf{x}+\mathbf{r})$, which is defined as the probability of finding a line segment with end points at $\mathbf{x}$ and $\mathbf{x}+\mathbf{r}$ entirely in phase 1 [10]. This function contains some connectedness information, at least along a lineal path, and hence reflects certain long-range information about the system. In an isotropic medium, the lineal-path function depends only on the distance r between the two end points and can be expressed simply as $L(r)$. Clearly, for all media having a volume fraction of ϕ_1,

$$L(0)=S_2(0)=\phi_1. \tag{11}$$

To evaluate $L(r)$ in a digitized system, it is again sufficient to let r take on integer values; sampling is again performed only along orthogonal directions [7]. In this respect, the sampling procedure to evaluate L reduces merely to a problem of identifying the lengths of the chords of the corresponding phase in the system. Provided the system is isotropic, this method of determining L is considerably more efficient than throwing random lines into the system.

C. Pore-size distribution and cumulative pore-size distribution function

The pore-size distribution function [11] $P(\delta)$ is defined in such a way that $P(\delta)d\delta$ is the probability that a randomly chosen location in the pore phase (phase 1 here) lies at a distance between δ and $\delta+d\delta$ of the nearest point on the pore-solid interface. The function $P(\delta)$ can be obtained only from a three-dimensional representation of the structure, as it contains *connectedness information about spherical regions in the pore space* [12]. Some useful properties of this function are

$$\int_0^\infty P(\delta)d\delta=1 \quad \text{and} \quad P(\infty)=0, \tag{12}$$

with

$$P(0)=\frac{s}{\phi_1}, \tag{13}$$

where s is the specific surface as defined above. The mean pore size is defined by the first moment of $P(\delta)$, i.e.,

$$\langle\delta\rangle=\int_0^\infty \delta P(\delta)d\delta. \tag{14}$$

The quantity $\langle\delta\rangle^2$ provides a lower bound on the mean survival time τ associated with a Brownian particle diffusing through the pore phase of a system of traps (see Sec. II E).

The cumulative distribution function $F(\delta)$ associated with $P(\delta)$ is defined as

$$F(\delta)=\int_\delta^\infty P(z)dz, \tag{15}$$

with

$$F(0)=1 \quad \text{and} \quad F(\infty)=0. \tag{16}$$

$F(\delta)$ is the fraction of pore space that has a pore diameter greater than δ. The mean pore size may also be defined in terms of the cumulative pore-size distribution function

$$\langle \delta \rangle = \int_0^\infty F(\delta) d\delta. \tag{17}$$

In evaluating the pore-size distribution function $P(\delta)$ in a 3D digitized medium, random points are thrown into the system and, for each point, the smallest distance from the point to the nearest pore-solid interface is recorded. The quantity $P(\delta)$ is then obtained by binning these distances and dividing by the total number of sampled distances. The mean pore size $\langle \delta \rangle$ is calculated simply by averaging these distances. The cumulative pore-size distribution function $F(\delta)$ is obtained by taking the list of the distances and incrementing all counters associated with distances less than or equal to a given distance. In the end, all counters are divided by the total number of distances. This method of using a list of distances closely parallels the method used to determine the lineal-path function.

D. Percolating volume fraction

Pore regions can either be disconnected or percolating between two ends of a medium. The fraction of the pore region that percolates over the total volume of the medium, denoted by ϕ_1^*, provides important morphological information. Unlike the volume fraction, this quantity is an intrinsically 3D quantity which cannot be obtained without a 3D representation of the medium as it contains *the degree of connectedness* of the pore space. The quantity ϕ_1^* can be evaluated efficiently by a ''burning algorithm'' for digitized media [13]. One starts by choosing the pore-phase pixels at one end of the system. These pore-phase pixels are then ''burnt,'' and their surrounding neighbors which have the same phase are iteratively burnt. The burning process continues until there is no more accessible unburnt pixels. If the ''fire'' reaches the opposite end of the system, then a continuous cluster of the pore phase exists, and these burnt pixels are marked as percolating pixels. The percolating fraction of porosity $f_p = \phi_1^*/\phi_1$ is easily evaluated from the number of the percolating pixels. This quantity measures the degree to which the pore space is percolating in the porous medium.

E. Mean survival time and fluid permeability

We consider estimating two important transport properties of the sandstone: the mean survival time τ and the fluid permeability k. The mean survival time τ (obtainable from a nuclear magnetic resonance experiment [14–16]) is the average time a Brownian or diffusing particle takes to diffuse in a trap-free region (with diffusion coefficient D) in a system of partially absorbing traps before it becomes absorbed by the trapping phase. Therefore, the quantity τD, which has a dimension of *(length)*^{2}, is intimately related to the characteristic length scale of the pore space. We will hereafter refer to τD as the ''*scaled* mean survival time.'' The quantity τ is also equal to the inverse of the trapping rate in diffusion-controlled reactions, which arise in a host of phenomena in the physical and biological sciences. It was shown to be rigorously bounded from below in terms of the mean pore-size $\langle \delta \rangle$ via the relation [17]

$$\tau \geqslant \langle \delta \rangle^2 / D. \tag{18}$$

In the Fontainebleau sandstone system that we consider, the void phase is identified with the trap-free region, and the grain phase is identified with the trap region. The mean survival time is measured by simulating the Brownian motion of diffusing particles in the void phase. The time for each particle to diffuse to the void-grain boundary is measured for each particle, and then averaged over all such particles. We use an efficient first-passage time algorithm first developed for continuum materials by Torquato and Kim [18], and then adapted by Coker and Torquato [19] for digitized media. The latter researchers also showed that measurement of τ in a digitized medium provides a lower bound on the true continuum mean survival time.

The slow flow of an incompressible viscous fluid through porous media is often described by Darcy's law [20],

$$\mathbf{v} = -\frac{k}{\mu} \nabla p, \tag{19}$$

where $\mathbf{v}$ is the average velocity of the fluid flowing through the medium, k is the fluid permeability of the medium, μ is the dynamic viscosity of the fluid, and ∇p is the applied pressure gradient. Torquato [8] developed a rigorous cross-property relation that relates the fluid permeability k to the mean survival time τ:

$$k \leqslant \phi_1 \tau D. \tag{20}$$

Thus a measurement of the mean survival time provides an upper bound on the fluid permeability. Avellaneda and Torquato [21] derived the first rigorous equality connecting the permeability to the effective electrical conductivity σ_e of a porous medium containing a conducting fluid of conductivity σ_1 and an insulating solid phase,

$$k = \frac{L^2}{8\mathcal{F}}, \tag{21}$$

where $\mathcal{F} = \sigma_1/\sigma_e$ is the formation factor and L is a length parameter which is a weighted sum over the viscous relaxation times associated with the time-dependent Stokes equations.

Since it is difficult to obtain L^2 exactly, rigorous treatments can only provide bounds on L^2. It has been conjectured [22] that for isotropic media possessing an arbitrary but connected pore space, the following relation holds:

$$k \leqslant \frac{\tau D}{\mathcal{F}}. \tag{22}$$

In practice, the bound (22) overestimates the permeability by roughly a factor of the porosity ϕ_1. Accordingly, it has been proposed [23] that the approximate relation

$$k \approx \phi_1 \frac{\tau D}{\mathcal{F}} \tag{23}$$

should be accurate for a large class of porous media. This relation will be used to provide an estimate of the fluid permeability of the Fontainebleau sandstone, and will be compared to the experimental value.

III. FORMULATION OF THE RECONSTRUCTION PROCEDURE

The approach that we will use to reconstruct a 3D random medium is an extension of the procedure that we proposed in paper I for digitized media [7], and applied to reconstruct a variety of random media in one and two dimensions. This method is a variation of the simulated annealing method introduced by Rintoul and Torquato [6] to reconstruct dispersions of particles. It involves finding a state of minimum ''energy'' among a set of many local minima by interchanging the phases of the pixels in the digitized system. The energy is defined in terms of the squared difference of the reference and simulated correlation functions. Our reconstruction procedure has a number of useful features: it is (i) simple to implement, (ii) generally applicable to multiphase and anisotropic structures, and (iii) able to include any type and number of correlation functions as microstructural information. In the interest of completeness, we will briefly outline the procedure for reconstructing an isotropic two-phase medium using the two-point probability function S_2 and the lineal-path function L as the morphological input. For a more detailed description of the general methodology, we refer the reader to paper I [7].

Consider reconstructing a medium where the ''reference'' correlation functions $f_o^{(k)}(r)$ are given information (the superscript k identifies the different correlation functions that are being used). In this study, we could identify $f_o^{(1)}(r)$ with the two-point probability function S_2, and $f_o^{(2)}(r)$ with the lineal-path function L of the reference medium. We will refer to the reconstruction procedure that uses only S_2 as the input microstructural information for the ''S_2 reconstruction,'' and the one that uses *both* S_2 and L as the ''hybrid reconstruction.'' The superscript k is therefore equal to 1 in the former case, and $k=[1,2]$ in the latter. To begin the reconstruction process, an initial guess of the system configuration is made. Without loss of generality, we use the 3D random checkerboard with the same volume fraction ϕ_1 of the reference system as the initial structure. This structure is constructed by randomly choosing the correct number of pixels according to the volume fraction of the system and assigning phase 1 to them.

Now let $f_s^{(k)}(r)$ be the corresponding correlation functions of the reconstructed digitized system at some time step during the reconstruction process. It is this system that we shall attempt to evolve toward the reference structure from the initial system configuration. Once the $f_s^{(k)}(r)$ at a particular time step are evaluated, a variable E which plays the role of the ''energy'' in the simulated annealing can be calculated as

$$E=\sum_k \sum_i [f_s^{(k)}(r_i)-f_o^{(k)}(r_i)]^2. \tag{24}$$

To evolve the digitized system toward the reference medium (or in other words, to minimize E), we interchange the states of two arbitrarily selected pixels of different phases. This phase interchange procedure has the nice property of automatically preserving the volume fraction of both phases during the reconstruction process. After the interchange is performed, we can calculate the energy E' of the resulting state and the energy difference $\Delta E=E'-E$ between two successive states of the system. This phase interchange is then accepted with probability $p(\Delta E)$ via the Metropolis method as

$$p(\Delta E)=\begin{cases} 1, & \Delta E\leqslant 0 \\ \exp(-\Delta E/T), & \Delta E>0, \end{cases} \tag{25}$$

where T is the ''temperature.'' This method causes $f_s^{(k)}(r)$ to converge gradually to $f_o^{(k)}(r)$, and is carried out successively until the evolving system's $f_s^{(k)}$ matches the reference $f_o^{(k)}$ within a tolerance limit. The cooling schedule, which governs the value and the rate of change of T, is chosen to allow the system to evolve to the desired state as quickly as possible, without getting trapped in any local energy minima. We adopt the suggestion that the starting T should have a value such that the initial acceptance rate is 0.5 [24]. Note that at the ground state, the energy E can be viewed as a *least-squares error* [25].

In paper I, we examined a diverse number of random model microstructures. The reconstructions generally captured the salient features of the reference systems, including the interfacial surface area [7]. However, even though the reference and reconstructed correlation functions were virtually identical, we found that the reconstructions deviated from the reference systems as measured by differences in other higher-order correlation functions of the system. This nonuniqueness is expected since lower-order correlation functions generally do not contain complete morphological information. Indeed, in Sec. I we showed (by way of examples) how different microstructures can have the same two-point function S_2. However, we note that since the ''energy'' that we use [Eq. (24)] is not a real Hamiltonian, it is highly nontrivial to elucidate quantitatively the selection mechanism that the simulated annealing uses to converge to the ground state.

We would like to note that in evaluating $f_s^{(k)}$ of the initial configuration, the sampling procedures described in Sec. II can be used. However, for the evolving structures generated during the reconstruction process, it is not necessary to sample the intermediate structures fully all over again by the same sampling methods to calculate the correlation functions. For instance, a change in S_2 from the previous structure is only due to the change of the success rate (the occurrence of the two end points fall in phase 1) along the rows or columns that cross each altered pixel. This change in S_2 can simply be evaluated by invoking the sampling technique *only* along those rows and columns crossing the altered pixels. Therefore, to evaluate the S_2 profile of a succeeding structure, S_2 of the preceding structure can be stored beforehand, and that of the subsequent structure can be updated efficiently by correspondingly adjusting the stored S_2 using the calculated change. This technique can similarly be applied to the lineal-path function evaluation: we only need to keep track of the length of the chords being destroyed and created due to the phase interchange of pixels, so that L can be efficiently updated according to these changes. This tech-

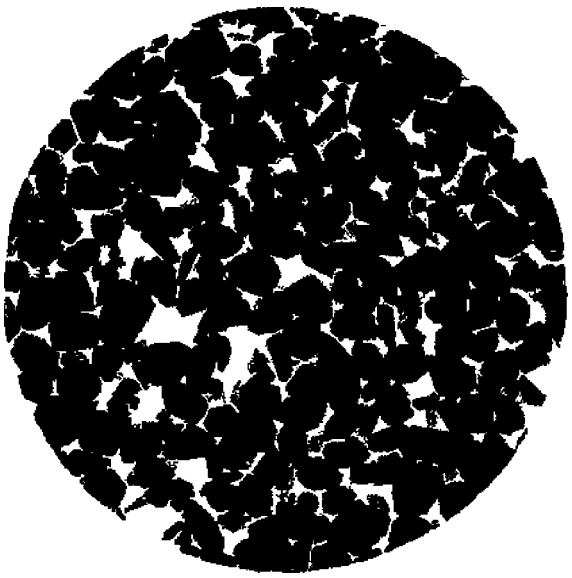

FIG. 1. Sample filtered slice of Fontainebleau sandstone. The white region corresponds to the pore phase. The diameter of the cylindrical core is 3 mm, with a pixel resolution of 7.5 μm.

nique should be exploited for any other correlation functions, whenever possible, in order to make the reconstruction algorithm more efficient.

IV. 3D RECONSTRUCTION OF FONTAINEBLEAU SANDSTONE

As stated in Sec. I, many morphological quantities for 3D isotropic media are obtainable exactly from 2D planes of the medium in the infinite-volume limit. What is not clear is the extent to which information contained in such correlation functions will be able to reproduce intrinsic 3D information, such as connectedness. We now address this issue by applying our reconstruction procedure to reconstruct a 3D Fontainebleau sandstone sample by measuring the two-point correlation function S_2 and lineal-path function L from 2D slices of the sample. These sections do not have periodic boundary conditions, and therefore sampling of the correlation functions are adjusted from those described in Sec. II accordingly.

A. Morphology and transport properties of sandstone

The tomographic image of the Fontainebleau sandstone sample we use is the same as that studied by Coker, Torquato, and Dunsmuir [26]. It consists of 300 planar slices separated by a distance of 7.5 μm, and each of the slices has dimensions of 512×512 pixels with a resolution of 7.5 μm per pixel. Therefore, the digitized image, which we will hereafter refer to as the ''reference'' sandstone image, consists of $512\times512\times300$ pixels, each of which constitutes a cubic region of size $7.5\times7.5\times7.5$ μm^3. The useful information of the sandstone is contained in a cylindrical region of around 420 pixels in diameter. A sample slice of the digitized sandstone is shown in Fig. 1. An image of a $128\times128\times128$ pixels subregion of the complicated 3D pore space and the 3D perspective of the surface cuts of the subregion is shown in Figs. 2(a) and 2(b), respectively.

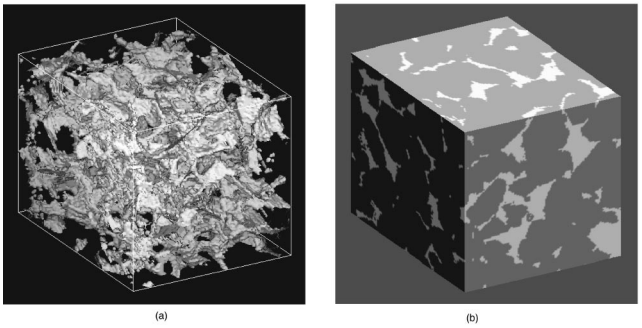

FIG. 2. (a) The pore space in a $128\times128\times128$-pixel subregion of the Fontainebleau sandstone. The pore space is white and opaque, and the grain phase is black and transparent. (b) 3D perspective of surface cuts of the subregion depicted in (a). The color code is the same as in (a).

As reported in Ref. [26], some of the internal slices were discarded due to experimental difficulties, reducing the number of useful slices to 296. In addition, the number of slices encompassing the largest region of the sandstone sample, where neighboring slices are not missing, is restricted to 211. When evaluating the structural quantities or the effective properties of the sandstone, we make use of these continuously run slices. Moreover, instead of extracting only a rectangular portion of the image as in Ref. [26] for data calculation, we retain and use all the useful information provided in the cylindrical region of the slices to give more reliable results.

We evaluate the morphological measures of the reference sandstone using the algorithms described in Sec. II. These results are summarized in Table I and Figs. 3–5. The correlation functions are found to be in close agreement with available experimental values [27]. The one-point probability function or the porosity ϕ_1 of the reference sandstone is found to be 0.1485, which is to be compared with the experimental measurement of 0.1484. The specific surface s of the reference sandstone is found to be 1.962×10^{-2} μm^{-1}. Corrected for the digitization effect using Eqs. (8) and (9), the specific surface becomes 1.541×10^{-2} μm^{-1}, which is to be compared with the experimental measurement of 1.546×10^{-2} μm^{-1}.

Certain intrinsically three-dimensional quantities, which are not obtainable from 2D cross-sectional images, are also evaluated. The percolating fraction of the pore space is found to be 98.8% by using the burning algorithm. The cumulative pore-size distribution function $F(\delta)$ is shown in Fig. 3. The mean pore size $\langle\delta\rangle$ and the scaled mean survival time τD are evaluated to be 6.47 μm and 89.11 μm^2, respectively. These 3D quantities will be compared to those of the reconstructed structures later. Employing these evaluated values and the rigorous lower bound of the formation factor $\mathcal{F}$ provided in Ref. [26] ($\mathcal{F}^{-1}\leqslant0.089$), the permeability of the sandstone is estimated by Eq. (23) to be 1.18 μm^2. This value is quite close to the experimental value of 1.3 μm^2 [27], thereby validating the reliability of the evaluated morphological quantities from the reference sandstone image.

B. Reconstruction results

To reconstruct the Fontainebleau sandstone, for purposes of efficiency, we take the target phase to be the pore phase

TABLE I. Morphological measures and effective properties of the reference and reconstructed Fontainebleau sandstone. The specific surface s is corrected for digitization effect by Eqs. (8) and (9). The permeability k is from the approximate relation (23).

Structure	Morphological measures ϕ_1	f_p (%)	s (10^{-2} μm^{-1})	$\langle\delta\rangle$ (μm)	Effective properties τD (μm^2)	k (μm^2)
Reference sandstone	0.1485	98.8	1.541	6.47	89.1	1.18
S_2 reconstruction:						
Slice 1	0.1464	84.7	1.575	5.87	71.6	0.93
Slice 2	0.1475	88.6	1.609	5.59	64.6	0.85
Slice 3	0.1476	86.2	1.564	5.83	71.4	0.94
Slice 4	0.1480	89.9	1.554	5.91	71.2	0.94
Hybrid reconstruction:						
Slice 1	0.1464	95.2	1.576	6.44	92.3	1.20
Slice 2	0.1475	91.2	1.611	6.66	89.8	1.18
Slice 3	0.1476	89.2	1.565	6.79	101.5	1.33
Slice 4	0.1480	94.5	1.555	6.51	89.3	1.18

since it has a lower volume fraction. The reconstructed structures have system sizes of $128\times128\times128$ pixels. We begin the reconstruction process by choosing a 2D slice of the tomographic image of the Fontainebleau sandstone, and then extract from it the structural functions S_2 and L for use in the reconstruction [28]. For illustration purposes, we provide here results of a few examples where the slices have approximately the same porosity as the reference sandstone (see columns 1 and 2 in Table I). The S_2 and L profiles obtained from these 2D slices are shown in Figs. 4 and 5. Note these profiles match closely the respective profiles of the original 3D image shown in the same figures. This validates that S_2 and L obtained from 2D slices represent well the correlation functions of the original 3D structure.

A typical S_2 reconstruction of the Fontainebleau sandstone is shown in Fig. 6 in 3D perspectives. While the 2D surface cuts of the reconstructed structure are not substantially different from the cuts of the reference sandstone [compare Figs. 6(b) and 2(b)], it is seen that the 3D pore topologies are not as close in appearance [compare Figs. 6(a) and 2(a)]. Visually, the hybrid reconstruction (see Fig. 7) provides a slightly better rendition of the true sandstone microstructure. The pore space of the reference sandstone is quite irregular in shape and size, containing ''platelike'' regions. By contrast, the complex pore spaces of the reconstructions do not appear to contain platelike regions, but rather are more globular in appearance. Note that in all of the reconstruction examples, the profiles of the *employed* correlation functions match the reference ones virtually exactly as shown in Figs. 8 and 9. Therefore, it can be misleading simply to compare the employed correlation functions and the 2D sections of the reference and reconstructed structures to validate the success of a reconstruction. As discussed in Refs. [6] and [7], nonuniqueness is expected due to the fact that lower-order correlation functions generally do not contain complete morphological information. Certainly, a more refined reconstruction can be produced by incorporating (in addition to the structural quantities that we have studied) higher-order morphological information [8]. However, from a practical point of view, it is important to realize that if the

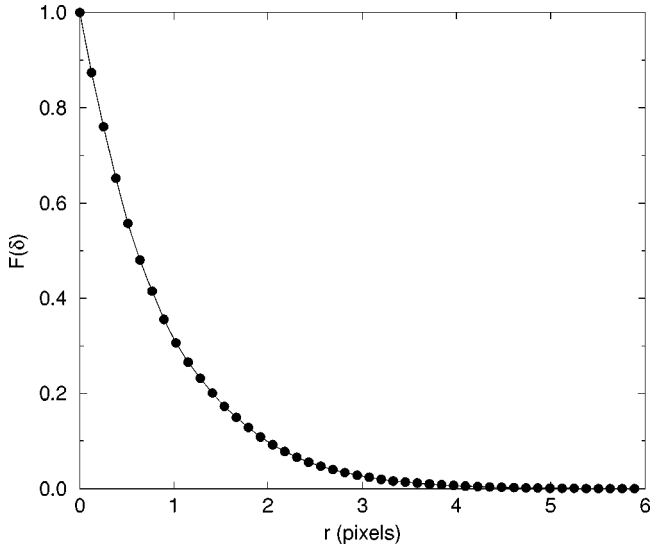

FIG. 3. Cumulative pore-size distribution function $F(\delta)$ of the Fontainebleau sandstone. One pixel is equal to 7.5 μm.

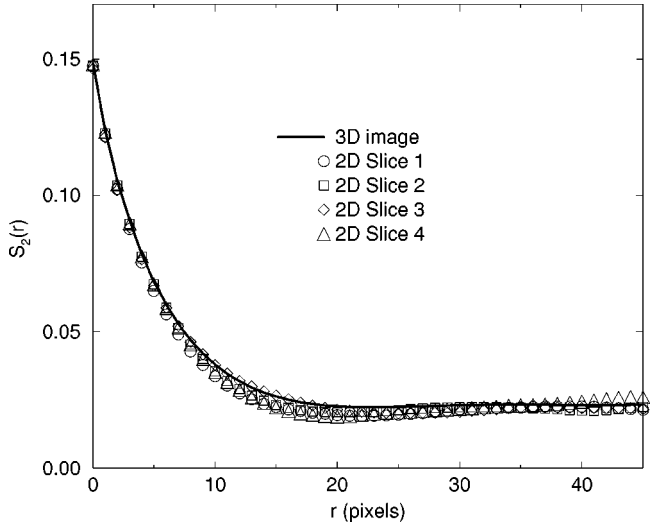

FIG. 4. Two-point probability function $S_2(r)$ of the Fontainebleau sandstone and the sample slices of the sandstone. One pixel is equal to 7.5 μm.

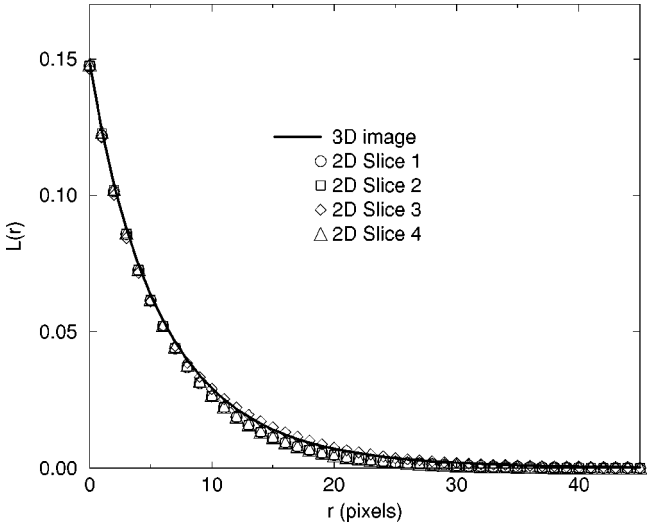

FIG. 5. Lineal-path function $L(r)$ of the Fontainebleau sandstone and the sample slices of the sandstone. One pixel is equal to 7.5 μm.

deemed crucial structural and effective properties of the reconstruction agree closely with that of the reference medium, then the reconstruction can be considered to be successful, *even if appearances suggest otherwise.*

Consequently, in order to judge whether the reconstructions are *quantitatively* successful, we will seek to measure and compare other important morphological measures and effective properties. The additional microstructural measures we choose for comparison include the percolating fraction of pore space f_p, specific surface area s, cumulative pore-size distribution $F(\delta)$, and the mean pore size $\langle \delta \rangle$. The percolating pore space is defined here as the pore space that is able to percolate through the medium from the three orthogonal faces as shown in Figs. 6(b) and 7(b) to the corresponding opposite faces. The effective properties such as the scaled mean survival time τD and the permeability k [as obtained from the approximate relation (23)] will also be compared. Except for the specific surface s, all of the aforementioned quantities are intrinsically three dimensional, and contain

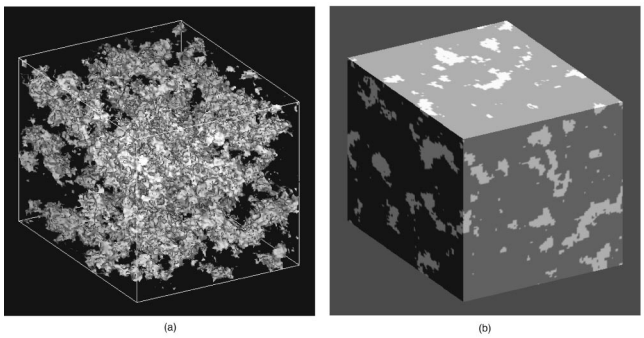

FIG. 6. S_2 reconstruction of the Fontainebleau sandstone using the two-point probability function S_2 obtained from slice 1. The system size is $128\times128\times128$ pixels, and one pixel is equal to 7.5 μm. (a) Pore space of the S_2 reconstruction. The pore space is white and opaque, and the grain phase is black and transparent. (b) 3D perspective of surface cuts of the reconstruction. The color code is the same as in (a).

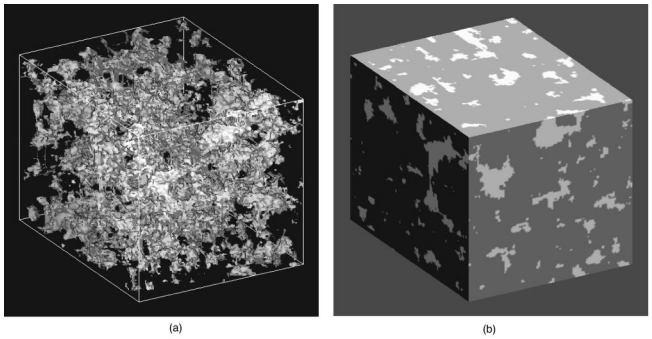

FIG. 7. Hybrid reconstruction of the Fontainebleau sandstone using a combination of the two-point probability function S_2 and the lineal-path function L obtained from slice 1. The system size is $128\times128\times128$ pixels, and one pixel is equal to 7.5 μm. (a) Pore space of the hybrid reconstruction. The pore space is white and opaque, and the grain phase is black and transparent. (b) 3D perspective of surface cuts of the reconstruction. The color code is the same as in (a).

some level of connectedness information about the pore space.

Table I compares the morphological quantities of the reference sandstone to those of the reconstructions. Figure 10 shows the cumulative pore-size distribution functions of the reconstructions from a typical slice, and the data for all other slices are very close to the shown data (and hence are not displayed). As expected, the specific surface s of all reconstructions match well with that of the reference sandstone since the S_2 profiles matches virtually exactly the reference ones [see Eq. (9) and note that s can be determined by the slope of $S_2(r)$ at $r=0$]. Also, it can be seen that all of the 3D morphological descriptors and effective properties of the reconstructions, especially those of the hybrid reconstructions, have very similar values to those of the reference sandstone. The S_2 reconstructions, however, are found generally to underestimate all of the measures that characterize the pore space, including the lineal-path function L (see Fig. 8) and the aforementioned 3D quantities. The hybrid recon-

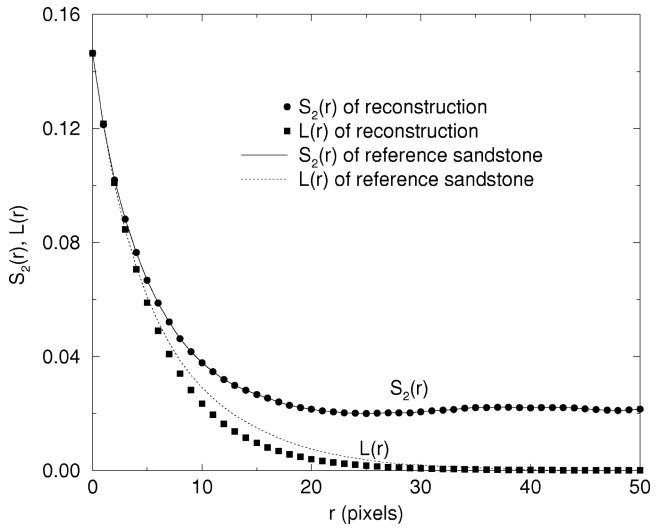

FIG. 8. S_2 of the reference sandstone and S_2 reconstruction from slice 1. Also shown is the lineal-path function L for both systems.

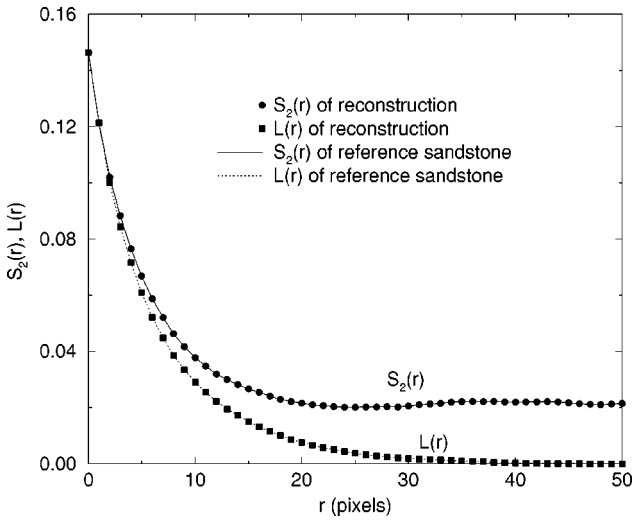

FIG. 9. S_2 and L of the reference sandstone and hybrid reconstruction from slice 1.

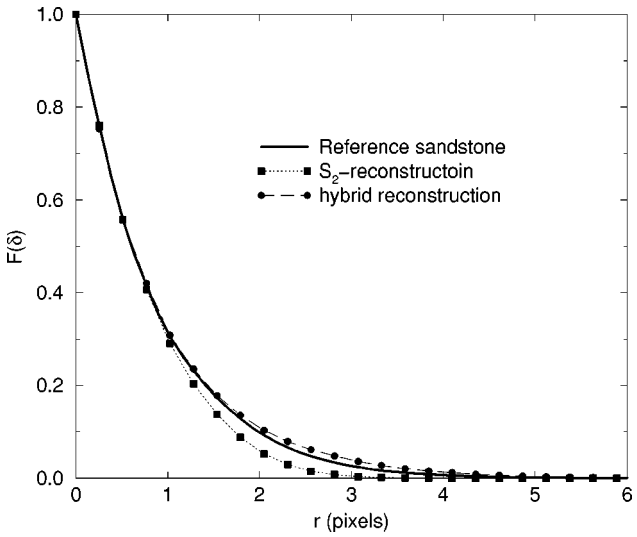

FIG. 10. Cumulative pore-size distribution function $F(\delta)$ for the reference Fontainebleau sandstone, S_2 reconstruction from slice 1, and the hybrid reconstruction from slice 1. One pixel is equal to 7.5 μm.

structions have correlation functions and effective properties that are strikingly similar to those of the reference sandstone, except for f_p, which will be commented on shortly. Note that the 3D quantities are more complicated functionally than the correlation functions that are being used for reconstruction, and they are derived only *indirectly* from the information obtained from the 2D images via the reconstruction process. Nonetheless, the 3D quantities of the hybrid reconstructions and the reference structure are remarkably similar, leading us to conclude that the correlation functions that we utilize in the hybrid reconstructions are sufficient to capture the relevant morphological information of the actual Fontainebleau sandstone.

The percolating fraction of the pore space f_p of the S_2 and hybrid reconstructions are on the average about 12% and 6% lower than that of the actual sandstone, respectively. These lower values of f_p indicate that the reconstructed structures have in general a lower degree of connectedness than that of the actual sandstone. Compared to the values of f_p, the hybrid reconstructions can be seen to capture better the degree of connectedness of the pore space than the S_2 reconstructions. Consequently, of the two methods of reconstruction, the hybrid reconstruction yields structures that more closely agree with all of the aforementioned intrinsically 3D morphological measures and effective properties of the reference sandstone. This confirms that the lineal-path function provides a level of connectedness information that S_2 does not have, albeit not sufficient to capture fully connectedness information. This shows that the reconstruction exercise can shed light on the nature of the information contained in the morphological quantities that are incorporated in the reconstruction process. This is invaluable in helping one to identify the appropriate quantities that can effectively characterize classes of structures.

V. CONCLUSIONS

For a random heterogeneous medium, intrinsically three-dimensional morphological measures such as the percolating pore space, pore-size distribution, mean pore size, mean survival time, and permeability are not obtainable directly from a two-dimensional image. However, one can make use of other structural measures which can be obtained exactly from the available 2D planes to reconstruct the medium in three dimensions. From the reconstructed 3D structure, intrinsically 3D quantities can subsequently be evaluated. Naturally, in order to produce an accurate reconstruction, one must utilize microstructural information which captures the salient features of the reference medium. We have developed and employed a reconstruction method that can incorporate any type and number of correlation functions, and specifically applied it to reconstruct a 3D Fontainebleau sandstone sample. We showed that it is sufficient to incorporate both the two-point probability function S_2 and the lineal-path function L (obtained from the 2D cross sections) for the reconstruction in order to reproduce accurately certain 3D morphological measures and macroscopic properties of the sandstone.

Of course, since S_2 and L contain only limited morphological information, such a reconstruction will not capture fully every feature of the reference medium. However, higher-order correlation functions [8] can easily be incorporated in our reconstruction if one desires a more refined reconstruction. Indeed, it is expected that for other classes of random media, other morphological quantities will be needed to capture the salient features. The sandstone reconstruction we carried out here sheds light on the nature of the information contained in the structural quantities that we implemented. This exercise is useful in identifying appropriate morphological descriptors that can effectively characterize different classes of structures.

ACKNOWLEDGMENTS

We would like to thank Rudolf Held for his help in rendering the three-dimensional images in this paper. We gratefully acknowledge the support from the U.S. Department of Energy, Office of Basic Energy Sciences, under Grant No. DE-FG02-92ER14275.

[1] J. A. Quiblier, J. Colloid Interface Sci. **98**, 84 (1984).
[2] P. M. Adler, C. G. Jacquin, and J. A. Quiblier, Int. J. Multiphase Flow **16**, 691 (1990); P. M. Adler, C. G. Jacquin, and J. F. Thovert, Water Resour. Res. **28**, 1571 (1992); P. M. Adler, *Porous Media: Geometry and Transport* (Butterworth-Heinemann, Boston, 1992); J. Yao, P. Frykman, F. Kalaydjian, J. F. Thovert, and P. M. Adler, J. Colloid Interface Sci. **156**, 478 (1993); J. Poutet, D. Manzoni, F. Hage-Chehade, C. G. Jacquin, M. J. Boutéca, J. F. Thovert, and P. M. Adler, Int. J. Rock Mech. Min. Sci. Geomech. Abstr. **33**, 409 (1996).
[3] A. P. Roberts and M. Teubner, Phys. Rev. E **51**, 4141 (1995); A. P. Roberts and M. A. Knackstedt, *ibid.* **54**, 2313 (1996); A. P. Roberts, *ibid.* **56**, 3023 (1997).
[4] P. Debye, H. R. Anderson, Jr., and H. Brumberger, J. Appl. Phys. **28**, 679 (1957).
[5] P. Levitz (unpublished).
[6] M. D. Rintoul and S. Torquato, J. Colloid Interface Sci. **186**, 467 (1997).
[7] C. L. Y. Yeong and S. Torquato, Phys. Rev. E **57**, 495 (1998).
[8] S. Torquato, Appl. Mech. Rev. **44**, 37 (1991).
[9] J. G. Berryman and S. C. Blair, J. Appl. Phys. **60**, 1930 (1986).
[10] B. Lu and S. Torquato, Phys. Rev. A **45**, 922 (1992).
[11] A. E. Scheidegger, *The Physics of Flow Through Porous Media* (University of Toronto, Toronto, 1974).
[12] S. Torquato, Physica A **207**, 79 (1994).
[13] D. Stauffer, *Introduction to Percolation Theory* (Taylor and Francis, London, 1985); see also E. J. Garboczi, M. F. Thorpe, M. DeVries, and A. R. Day, Phys. Rev. A **43**, 6473 (1991).
[14] J. R. Banavar and L. M. Schwartz, Phys. Rev. Lett. **58**, 1411 (1987).
[15] D. J. Wilkinson, D. L. Johnson, and L. M. Schwartz, Phys. Rev. B **44**, 4960 (1991).
[16] J. H. Strange, M. Rahman, and E. G. Smith, Phys. Rev. Lett. **71**, 3589 (1993).
[17] F. A. L. Dullien, *Porous Media* (Academic, London, 1979).
[18] S. Torquato and M. Avellaneda, J. Chem. Phys. **95**, 6477 (1991).
[19] S. Torquato and I. C. Kim, Appl. Phys. Lett. **55**, 1847 (1989).
[20] D. A. Coker and S. Torquato, J. Appl. Phys. **77**, 6087 (1995).
[21] M. Avellaneda and S. Torquato, Phys. Fluids A **3**, 2529 (1991).
[22] S. Torquato and I. C. Kim, J. Appl. Phys. **72**, 2612 (1992).
[23] L. M. Schwartz, N. Martys, D. P. Bentz, E. J. Garboczi, and S. Torquato, Phys. Rev. E **48**, 4584 (1993).
[24] M. P. Allen and D. J. Tildesley, *Computer Simulation of Liquids* (Clarendon, Oxford, 1987).
[25] We choose a cooling schedule such that the temperature decreases by 1% after 10 000 phase interchanges (successful or not). The algorithm terminates either when the energy E [defined by Eq. (24)] is less than some small tolerance value, or when the number of consecutive unsuccessful phase interchanges is greater than 100 000.
[26] D. A. Coker, S. Torquato, and J. H. Dunsmuir, J. Geophys. Res. **101**, 17 497 (1996).
[27] L. M. Schwartz, F. Auzerais, J. Dunsmuir, N. Martys, D. P. Bentz, and S. Torquato, Physica A **207**, 28 (1994).
[28] It should be noted, however, that in most applications, only a single slice is available, and hence in such cases one does not have the luxury of selecting different slices.